Identifying Critical Use Cases for a Plug-in Hybrid Electric Vehicle Battery Pack from Thermal and Ageing Perspectives

2021-01-1251

Identifying critical use cases for a plug-in hybrid electric vehicle battery pack from thermal and ageing perspectives

Marco Del Prete, Pier Giuseppe Anselma, Giovanni Belingardi
Department of Mechanical and Aerospace Engineering (DIMEAS), Politecnico di Torino, Torino, Italy
Center for Automotive Research and Sustainable Mobility (CARS), Politecnico di Torino, Torino, Italy

Abstract

The current trend towards an increasing electrification of road vehicles brings to life a whole series of unprecedent design issues. Among these, the ageing process that affects the lifetime of lithium-ion based energy storage systems is of particular importance since it turns out to be extremely sensitive to the variation of battery operating conditions normally occurring especially in hybrid electric vehicles (HEVs). This paper aims at analyzing the impact of operating conditions on the predicted lifetime of a parallel-through-the-road plug-in HEV battery both from thermal and ageing perspectives. The retained HEV powertrain architecture is presented first and modeled, and the related energy management system is implemented. Dedicated numerical models are also discussed for the high-voltage battery pack that allow predicting its thermal behavior and cyclic ageing. A wide variety of operating conditions is subsequently simulated including different driving scenarios, ambient temperatures, vehicle payloads, and battery state-of-charge (SOC) conditions. Obtained results highlight considerable impacts of the HEV operating conditions on the battery lifetime even in the advised operating temperature interval ranging from 15°C to 35°C. Moreover, charge-depleting HEV operation and high ambient temperature are identified as the most influencing conditions concerning the criticality of the use case. On the other hand, vehicle payload and specific driving scenario appear to have a reduced impact. Presented results might help engineers to improve the effectiveness of current high-voltage battery temperature control systems to extend the battery lifetime while ensuring improved energy economy.

Introduction

Nowadays, the inclination towards a continuous reduction in the automotive environmental impact finds a valuable ally in both hybrid electric vehicles (HEVs) and battery electric vehicles (BEVs), generally indicated as xEVs [1]. Nevertheless, the consequent introduction of Li-Ion energy storage systems (ESSs), which are currently the most employed electrochemical solution [2], brings along some critical issues that restrict the diffusion of electrified powertrains. However, if the consequent higher cost of xEVs might be mitigated by a great deal of governmental incentives, the current limited amount of km drivable in pure electric mode has led the market to prefer HEVs on BEVs in the latest years [1]. In particular, among the successful HEVs, the plug-in solution (PHEV) is noteworthy since it bridges the gap between the different types of xEVs [2]. Nonetheless, similarly to the other electrified vehicles, PHEV batteries as well incur the cycle ageing process [2] that affects Li-Ion ESSs and whose magnitude, contrary to the calendar ageing [2], is largely influenced by battery operating conditions, namely temperature, C-rate and depth-of-discharge (DOD). Among these, temperature is known to be an extremely impacting parameter on battery cycle ageing [2,3]. Nevertheless, vehicle-level HEV simulation tools developed in literature generally assume that the battery temperature is ideally maintained constant over time by the conditioning system [4,5]. This may represent a strong assumption since the real-world battery temperature might vary considerably, thus heavily impacting on battery ageing phenomena. In this paper, the impact of temperature on ageing has been consequently analyzed by simulating a quasi-static model [6] of a PHEV. The simulated PHEV layout has been inspired by the *Jeep® Renegade 4xe* [7] and it is equipped with a rule-based (RB) energy management strategy (EMS). Differently from other works exploring temperature impact on ESSs ageing [8,9], several driving missions (including some real-world ones), various payload conditions and different ambient temperatures have been assessed. MATLAB® and Simulink® software has been employed to this end. The organization of this paper is the following one: the *Renegade 4xe* powertrain, the retained RB EMS and the quasi-static modeling approach (QSA) are described first. Adopted methodologies for modelling the battery from electrical, thermal and ageing perspectives are then described. Afterward, the simulated plug-in HEV use cases are specified. Obtained results are commented and conclusions are finally given.

Retained HEV Powertrain

As illustrated in Figure 1, the powertrain designed for the *Renegade 4xe* adopts a parallel-through-the-road plug-in HEV configuration and it is equipped with a 1.3-liter, four-cylinder, turbocharged spark-ignition internal combustion engine (ICE) [7] acting on the front axle. Two permanent magnet electric generator\motors are embedded, one in configuration P4 (at the rear axle) and one in configuration P0 as belt starter-generator, from now on respectively indicated as MGP4 and MGP0. Concerning the high-voltage (HV) battery, it is undoubtedly the most critical element of the entire vehicle. Although the next section will provide further information about this crucial electrochemical component, it is fundamental to inform the reader that the HV battery analyzed in this study has not been considered made of $LiNiMnCoO_2$ (NMC) cells as in the actual *Renegade 4xe*, but of the largely investigated A123 26650 cells [10]. Specifically, this choice has been taken because both a widely accepted battery cycle ageing model and open-source data are available for this latter type of cell [5,10,11]. Obviously, this replacement has been performed with the constraint of obtaining overall battery characteristic values as close as possible to the real ones (11.4 kWh of nominal capacity and 400 V of nominal voltage [7]). Retained vehicle data are reported in Table 1, while further details concerning the on-board HEV RB EMS and the powertrain components are discussed in the follow-up of this section.

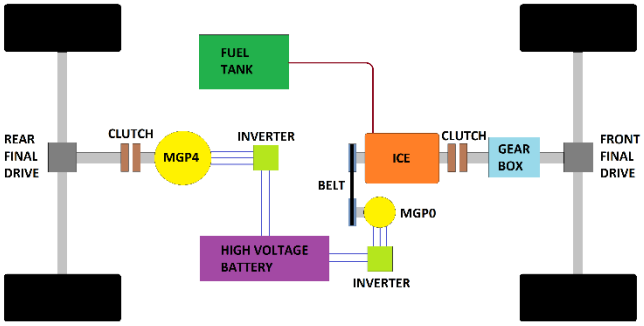

Figure 1. PHEV powertrain diagram.

Table 1. PHEV powertrain parameters.

Component	Parameter	Value
ICE	Max. power (hp @ RPM)	130 @ 5˙500
	Max. torque (Nm @ RPM)	270 @ 1˙850
MGP4	Max. power (hp @ RPM)	60 @ >1˙240
	Max. torque (Nm @ RPM)	250 @ <1˙240
MGP0	Max. power (hp @ RPM)	20 @ >2˙480
	Max. torque (Nm @ RPM)	48 @ <2˙480
Transmission ratios	Rear final drive (-)	10
	Front final drive (-)	4.438
	Automatic transmission (-)	[4.15; 2.12; 1.36; 0.98; 0.76; 0.62]
	MGP0 belt (-)	2.7
	Wheel radius (m)	0.322
HV battery	Battery nominal values (kWh/V)	10.94/400
	Cell nominal values (kWh/V)	3.33/7.6
	Pack configuration	120 S;12 P
	Cell type	A123 ANR26650
Vehicle	Road load coefficient A (N)	94.035
	Road load coefficient B (Ns/m)	3.805
	Road load coefficient C (Ns^2/m^2)	0.476

HEV On-board Control Logic

The considered HEV embeds an ICE, a MGP0 and a MGP4. These three power components allow the HEV to drive in three different operating modes as specified by the vehicle manufacturer [7]. These include:

1. Electric mode (mode1), in which the traction is provided by the MGP4 only;
2. Hybrid mode (mode2), which is characterized by the three power components being controlled in order to have the ICE working close to its optimal operating line (OOL) and not beyond, i.e. the values of ICE torque maximizing the engine efficiency for each given value of ICE rotational speed;
3. E-save mode (mode3), where the ICE can be simultaneously employed for propelling the HEV and charging the battery by means of the MGP0 working as a generator.

Moreover, all the operating modes allow performing regenerative braking. Before or during the trip, the driver can manually select either one of the three operating modes. However, the operating mode selected by the driver might not always correspond with the actual electrified powertrain operation since the RB supervisory controller implemented in the PHEV might automatically switch to a more appropriate operating mode. This might occur as example due to the battery operation not complying with state-of-charge (SOC) or to driver's power demand exceeding power limits of the electric machines. SOC and power values are therefore constantly monitored by the RB controller while driving; however, as suggested by numerical results presented in this paper, battery temperature should affect the operating mode selection as well in order to safeguard this component lifetime. The RB HEV controller implemented in this study operates as follows:

- when the Electric mode (i.e. mode1) is selected, an automatic shift to Hybrid mode (i.e. mode2) is performed if the SOC goes below 0.30 to preserve battery charge sustenance. Moreover, if the driver's power demand exceeds for a given time instant the value that can be provided by the MGP4 alone in Electric mode, the powertrain temporarily operates in Hybrid mode.
- when the Hybrid mode is selected, the RB HEV controller keeps pure electric operating mode in any case if battery SOC is higher than 0.60. The Hybrid mode is then activated as the battery SOC falls below 0.60. In case the battery SOC falls below 0.25, the RB HEV controller switches to the E-save mode to charge the battery until SOC reaches 0.30, returning then to Hybrid mode;
- when selected, the E-save mode (i.e. mode3) is operated only if the SOC is lower than 0.70. On the other hand, if SOC is higher than 0.70, the RB HEV controller operates in Hybrid mode. When the battery SOC falls below 0.70, and E-save mode is in operation, the battery is charged up to 0.80 before switching to Hybrid mode again.

HEV Modelling Approach

Moving on, the already mentioned QSA has been adopted for modelling the HEV. QSA is largely used for HEV powertrain design and analysis thanks to its high computational efficiency [6]. On one hand the employment of lookup tables lets the powertrain to be modelled in a simple stationary way, on the other hand QSA implies an inversion of the usual cause-and-effect relationship in evaluating speeds and torques of power components from the driver's power demand. A proportional–integral–derivative (PID) controller is introduced here to model the driver following the speed profile over time for given drive cycles. As far as the lookup tables employed in this paper are concerned, they are illustrated in Figure 2 and they have been generated using dedicated tools in Amesim® software that follow mathematical procedures available in literature [12,13].

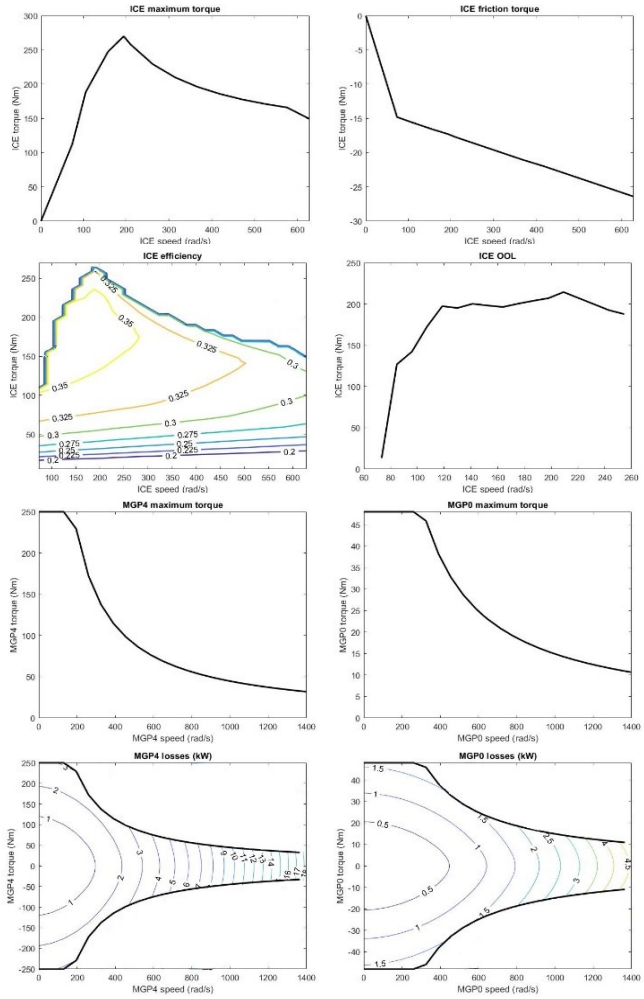

Figure 2. Motors lookup tables.

The total vehicle resistive force $F_{res,tot}$ (N) can be easily computed from the vehicle free body diagram using equation (1):

$$F_{res,tot} = F_{aero} + F_{roll} + F_{misc} + F_{grad} \ (1)$$

where F_{aero} is the aerodynamic drag, F_{roll} represents the rolling resistance, F_{misc} incorporates some miscellaneous terms whereas F_{grad} is the grading resistance related to road slope angle ϑ. Specifically, the aforesaid resistive terms have been evaluated as follows:

$$F_{aero} + F_{roll} + F_{misc} = A + Bv + Cv^2 \ (2)$$

$$F_{grad} = m_{veh} g sin\vartheta \ (3)$$

where A, B and C are the vehicle road load coefficients [5], v is the longitudinal speed of the vehicle, g represents the gravitational acceleration, m_{veh} is the total mass of the vehicle in kilograms, that is assumed here related to the number of passengers n_{pass}:

$$m_{veh} = 1768 + 100 \cdot n_{pass} \ (4)$$

By introducing the tractive or braking force F_{pwt} provided at the wheels by the powertrain, the equilibrium equation of the system can be written as:

$$m_{veh} a = F_{pwt} - F_{res,tot} \ (5)$$

where a indicates the longitudinal acceleration of the vehicle. Moving to the HEV driveline, the total powertrain torque T_{pwt} requested at the wheels can be computed as:

$$T_{pwt} = F_{pwt} r_{wheel} \ (6)$$

in which r_{wheel} is the radius of the wheels. By expliciting then all possible contributions to T_{pwt}, equation (7) is obtained:

$$T_{pwt} = T_{ICE,wheel} + T_{MGP4,wheel} + T_{MGP0,wheel} - T_{brakes} \ (7)$$

in which the terms $T_{ICE,wheel}$, $T_{MGP4,wheel}$ and $T_{MGP0,wheel}$ represent the values of torque provided at the wheels by the different power components according to RB EMS. T_{brakes} is the torque supplied by the brakes.

With respect to the torques T_{ICE}, T_{MGP4} and T_{MGP0} effectively outputted by the power components, they are evaluated backwardly from previous torques at the wheels by means of relations using transmission ratios collected in Table 1 and appropriate efficiencies [14]. The wheel angular speed ω_{wheel} can be defined as follows.

$$\omega_{wheel} = \frac{v}{r_{wheel}} \ (8)$$

Multiplying by transmission ratios it is then possible to introduce ω_{MGP4} , ω_{ICE} and ω_{MGP0} that represent angular speeds of MGP4, ICE and MGP0, respectively. Once the operating conditions (i.e. torque and speed) of each power component are known, it is possible to evaluate the fuel consumed by the ICE and the electric power requested by the electric motors to the HV battery. This is performed by means of the lookup tables reported in Figure 2. Therefore, the following equations can be written:

$$M_{fuel} = \int_0^t \dot{m}_{fuel} \, dt + n_{crank} m_{crank} \ (9)$$

$$P_{bat,MGP4} = \omega_{MGP4} T_{MGP4} + P_{loss,MGP4} \ (10)$$

$$P_{bat,MGP0} = \omega_{MGP0} T_{MGP0} + P_{loss,MGP0} \ (11)$$

In which M_{fuel} is the total quantity of fuel in grams consumed by the ICE up to time instant t, $\dot{m}_{fuel}$ is the fuel consumption rate in grams per second, m_{crank} is the mass of fuel required to crank the ICE (equal to 0.5 grams here), n_{crank} enumerates how many times the ICE is cranked over time, $P_{bat,MGP4}$ and $P_{bat,MGP0}$ are respectively the powers requested or supplied by the electric motors to the battery, whereas $P_{loss,MGP4}$ and $P_{loss,MGP0}$ indicate the power losses that characterize the two electric motors.

Battery Ageing and Thermal Model

In this work, a complete overview of the HV battery has been achieved by adopting the following methodologies:

1. an equivalent circuit model (ECM) [15] for battery electrical modelling;
2. a single temperature lumped-parameter model in order to evaluate battery temperature evolution during HEV operation;
3. a throughput-based battery capacity fade model [11] to evaluate battery cycle ageing.

Each of the listed modeling methodologies will be illustrated in the follow-up of this section.

Equivalent Circuit Model

The battery pack ECM is illustrated in Figure 3 and it has been obtained considering an A123 cell equivalent circuit and applying Thevenin's theorem to the pack configuration declared in Table 1.

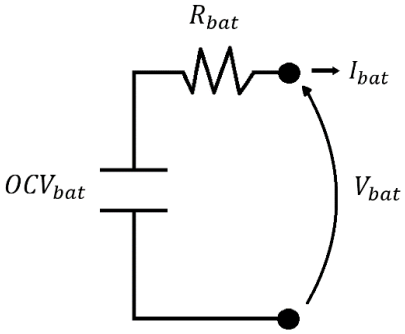

Figure 3. Battery equivalent circuit model.

In particular, the following equations hold:

$$OCV_{bat} = N_s OCV_{cell} \quad (12)$$

$$R_{bat} = \frac{N_s}{N_p} R_{cell} \quad (13)$$

where N_s and N_p are respectively the number of cells in series per branch and the number of parallel branches, OCV_{cell} and OCV_{bat} represent open circuit voltages of one single cell and of the HV battery pack, whereas R_{cell} and R_{bat} are the internal resistances of cell and pack, respectively.

Analogous considerations have been made for cell and battery pack capacities C_{cell} and C_{bat}, linked as in equation (14) when expressed in Ah:

$$C_{bat} = N_p C_{cell} \quad (14)$$

By applying then the power conservation law to battery ECM and by introducing battery power P_{bat} as calculable from powertrain operating condition and auxiliaries power demand, battery current I_{bat} can be computed by means of equation (15):

$$I_{bat} = \frac{OCV_{bat} - \sqrt{OCV^2{}_{bat} - 4P_{bat}R_{bat}}}{2R_{bat}} \quad (15)$$

However, when dealing with Li-Ion batteries, using C-rate c instead of I_{bat} is normally preferred since providing a more distinct information about battery exploitation, as perceivable from equation (16):

$$c = \frac{|I_{bat}|}{C_{bat}} \quad (16)$$

Consequently, after computing I_{bat}, battery state-of-charge SOC can be evaluated at any instant by knowing its value SOC_0 at the beginning of each driving mission and using the current integration method [4,5]:

$$SOC = SOC_0 - \int_0^t \frac{I_{bat}}{C_{bat}} dt \quad (17)$$

It should be noted that cell parameters are not constant, yet their values change during HEV operation. In particular, with respect to OCV_{cell}, its value varies with SOC, whereas R_{cell} depends on more factors, namely SOC, C-rate, battery temperature and charging/discharging condition [4,10,11]. OCV_{cell} is sensitive to temperature variation as well, yet its variation is normally of less impact.

Single Temperature Lumped-Parameter Model

Temperature is extremely impactful on battery lifetime. This especially holds when battery temperature falls beyond the ideal thermal thresholds, currently estimated within 15°C and 35°C [16]. In fact, in order to maintain as much as possible battery temperature in the ideal thermal range, ESSs are normally equipped with a battery thermal management system, including both cooling and heating systems [2,16]. With respect to this work, modelling these systems has not been considered to ease the clarity and meaning of obtained outcomes. Indeed, results will later demonstrate the importance of contrasting thermal variation with specific conditioning plants that must modelled in a realistic way, especially of cooling type. In general, the battery pack is an extended body characterized by a distribution of temperature values that is rather complex to model. Even if the single temperature lumped-parameter model takes into account one single battery temperature T_{bat}, it is largely employed [4,5,11] since considers a valid compromise between simplicity and accuracy. Moving on, the heat generated by the battery Q_{bat} can take two different paths: a portion Q_C remains stored in the battery and contributes to increase its temperature, while the remaining part Q_{air} is dispersed by means of natural convective phenomena with the surrounding air which has been set equal to ambient temperature T_a. As a consequence, equation (18) can be specified:

$$Q_{bat} = Q_C + Q_{air} \quad (18)$$

which, by expliciting each term, can be rewritten as:

$$R_{bat}{I_{bat}}^2 = m_{bat}c_{bat}\frac{dT_{bat}}{dt} + h_{air}S_{bat}(T_{bat} - T_a) \quad (19)$$

where m_{bat}, c_{bat} and S_{bat} refers respectively to battery mass, specific heat and exchange surface with the surrounding air, characterized by the convective coefficient h_{air}. All these thermal parameters are collected in Table 2. It should be noted that Q_{bat} in equation (19) has been considered related to Joule's heating only, as normally performed in literature, without taking into account temperature variation due to entropy changes [17].

Table 2. Battery and air thermal parameters.

m_{bat} (kg)	109.44
c_{bat} (J/(kgK))	1.1
S_{bat} (m^2)	1˙109.2
h_{air} ($W/(m^2K)$)	10

Throughput-based Battery Capacity Fade Model

Moving then to HV battery cycle ageing evaluation, a largely employed throughput-based battery capacity fade model has been used [11] that is calibrated for A123 26650 cells and based on the concept of battery charge throughput (Ah-throughput). Although the coexistence in literature of two divergent interpretations of Ah-throughput, here indicated as Q_{EOL}, the one including the impact of recharges on battery life [18] has been adopted in this work since more precautionary. Consequently, Q_{EOL} has been associated to the overall quantity of charge (in Ah) that a battery is able to process before reaching its end of life (EOL), calculable as:

$$Q_{EOL} = \int_0^{t_{EOL}} |I_{bat}| dt \quad (20)$$

where t_{EOL} is the instant of time in which EOL occurs. The value of t_{EOL} depends on the battery operating conditions. Conventionally, the EOL happens when the percentage value of battery nominal capacity faded, indicated by $C_{fade,\%}$, equals 20% (i.e. $C_{fade,\%} = 20$). When the battery operates under constant conditions, Q_{EOL} and $C_{fade,\%}$ can be evaluated by adapting to the entire battery the formula proposed in [11] for a single A123 26650 cell, inspired by the Arrhenius' gas equation [3] and employable for battery temperature between 15°C and 60°C only:

$$C_{fade,\%} = B \cdot exp\left(-\frac{A_f}{T_{bat}}\right)\left(\frac{Q_{EOL,const}}{N_p \cdot 1Ah}\right)^z \quad (21)$$

where battery Ah-throughput has been indicated as $Q_{EOL,const}$ to specify that it refers to constant operating conditions. In equation (21) are then present the terms B, A_f and z, which are reported in Table 3 and indicate respectively the pre-exponential, the ageing and the power-law factors [5]. Since these parameters refer to a single cell, $Q_{EOL,const}$ has been divided by the number of parallel branches N_p in order to scale to the whole battery pack.

Table 3. Battery ageing parameters for A123 26650 cell.

B	c=0.5	31˙630
	c=2	21˙681
	c=6	12˙934
	c=10	15˙512
A_f (K)		3˙814.68-44.56c
z		0.55

Moreover, as B and A_f vary along with battery C-rate, $Q_{EOL,const}$ depends on both the operating conditions T_{bat} and C-rate, as shown in Figure 4. However, the larger capacity of PHEV batteries slightly reduces the overall values of C-rate and it implies that the variation in $Q_{EOL,const}$ might largely relate to thermal aspects. Looking again at Figure 4, thermal phenomena might have a considerable influence even when the battery temperature remains within the ideal range of 15°C to 35°C.

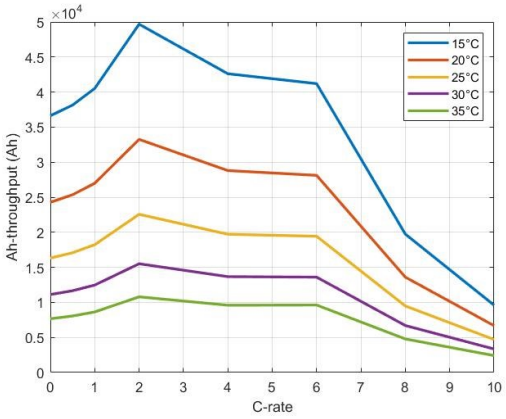

Figure 4. Ah-throughput variation with the operating conditions.

After calculating $Q_{EOL,const}$ from equation (21), the overall quantity of charge Q_{const} supplied by the battery under fixed values of C-rate and temperature is known. Then, it is possible to evaluate the current battery ageing state by comparing Q_{const} with $Q_{EOL,const}$. However, since batteries employed in HEVs are characterized by continuously changing operations, the contribution of each combination of C-rate and T_{bat} towards the achievement of Q_{EOL} over time can be evaluated by integrating the instantaneous state-of-health (SOH) variation:

$$SOH = SOH_0 - \int_0^t \frac{|I_{bat}|}{Q_{EOL,const}(c, T_{bat})} dt \quad (22)$$

where SOH_0 is the initial state-of-health of the battery and it is equal to 1 at the beginning of battery life.

Use Case Selection

As specified in the introductive section, the objective of this paper is to test the retained HV battery under a wide range of different operating conditions to provide inputs for developing effective battery sensitive HEV EMSs. Indeed, when investigating a wide range of different real-world battery operating conditions, it is advisable to exclude all the use cases of little significance for battery ageing. To this end, the impact of battery initial SOC and HEV operating mode selection on predicted battery lifetime has been examined. The results section will then consider different driving missions, climate conditions (i.e. ambient temperatures) and number of passengers.

Impact of Initial SOC and HEV Operating Mode

To assess the impact of initial SOC and HEV operating mode on battery temperature and lifetime, the Worldwide-harmonized Light Vehicle Test procedure (WLTP) has been simulated travelled by the HEV. The operating mode selected by the driver has been kept constant for the entire drive cycle, and twelve initial plug-in HEV use cases are defined combining each possible operating mode (i.e. mode1, mode2 and mode3) and four different values of SOC_0: 0.95 (i.e. battery completely charged), 0.70, 0.40 and 0.21. Moreover, a constant ambient temperature T_a equal to 25°C and only driver (n_{pass} =1) were considered. Using equation (22) and assuming that the initial battery state of health SOH_0 is equal to 1 for each possible combination of HEV operating mode and SOC_0 value, it is possible to

obtain the related final values of SOH, indicated as SOH_{end}. Results for a driving mission made of four WLTP repetitions are reported in Table 4.

Table 4. SOH_0 and SOH_{end} comparison when simulating 4 WLTP in series.

SOH_0 -SOH_{end} (10^5)		SOC_0			
		0.95	0.70	0.40	0.21
4x WLTP	mode1 (Electric)	14.6	10.2	4.86	3.74
	mode2 (Hybrid)	9.04	4.79	2.76	3.74
	mode3 (E-save)	6	3.71	7.06	9.2

In particular, from Table 4 it can be observed that the major difference among $\boldsymbol{SOH_0}$ and $\boldsymbol{SOH_{end}}$ occur when Electric mode is selected. This driving mode is clearly the one that exploits most battery operation. Moreover, the most critical ageing condition happens at $\boldsymbol{SOC_0}$=0.95, since, evidently, the battery is used longer for electric driving. Therefore, the most critical conditions of use of the battery occur when it is fully charged before the driving mission and the driver chooses Electric mode. Further considerations will therefore focus on this critical case.

Battery Kilometrical Lifetime Definition

To improve the clarity and ease of understanding for presented results, the equivalent vehicle mileage provided by the battery during its life is introduced. A reasonable and sufficient mileage that a battery should achieve during its lifetime amounts from 200 thousand kilometers to 300 thousand kilometers. The kilometrical battery lifetime is indicated here as $L_{bat,km}$ and it can be evaluated under the following assumptions:

1. when simulating a drive cycle continuously, the battery is assumed to be fully charged from the grid at the end of each mission;
2. the driving mission and the related final battery charge are supposed to be steadily repeated until the battery EOL is reached.

The following equation can then be defined:

$$L_{bat,km} = \frac{1}{1 - SOH_{end} + \Delta SOH_{rech}} \cdot s_{km,tot} \quad (23)$$

where SOH_{end} is computed by using equation (22) and it refers to the single driving mission, $s_{km,tot}$ is the total space travelled throughout the drive cycle in kilometers, ΔSOH_{rech} is the variation of battery SOH due to the plug-in charging from SOC_{end} back to SOC_0, that is supposed being performed at a constant battery temperature T_{rech} (equal to T_a if $T_a \geq 15°C$ and to 20°C otherwise) and with a C-rate equal to 2 to simulate fast charging. The initial value of T_{bat} is always set to T_{rech}. ΔSOH_{rech} can then be expressed as:

$$\Delta SOH_{rech} = \int_0^{t_{rech}} \frac{|I_{rech}|}{Q_{EOL,rech}(c_{easywall}, T_{rech})} dt \quad (24)$$

in which I_{rech} is the constant grid charging current, related to the grid charging C-rate $c_{easywall}$, $Q_{EOL,rech}$ is the battery Ah-throughput related to grid charging conditions T_{rech} and $c_{easywall}$. t_{rech} is the grid charging time duration in seconds and it can be calculated as:

$$t_{rech} = \frac{SOC_0 - SOC_{end}}{c_{easywall}} \quad (25)$$

Use Case Specifications

This sub-section provides specifications for a larger sample of vehicle potential operation that can be considered to investigate battery ageing behavior more exhaustively. Considered operating factors include driving condition, ambient temperature and payload. Eight different driving missions are considered including four standard drive cycles (WLTP, RTS 95, FTP 75 and HWFET) and four real-world driving cycles (RWCs). Namely, an extra-urban uphill mission (RWC01), a long highway trip (RWC03), a down mountain journey (RWC04) and an extra-urban downhill mission (RWC06). Specifically, RWCs have been recorded by means of global positioning system and their consideration increases the exhaustiveness of this study since road grade information is considered and not neglected as usually done in standard drive cycles. The main information about these eight driving missions is reported in Table 5, while the corresponding time series of vehicle speed and net road altitude over time are illustrated in Figure 5.

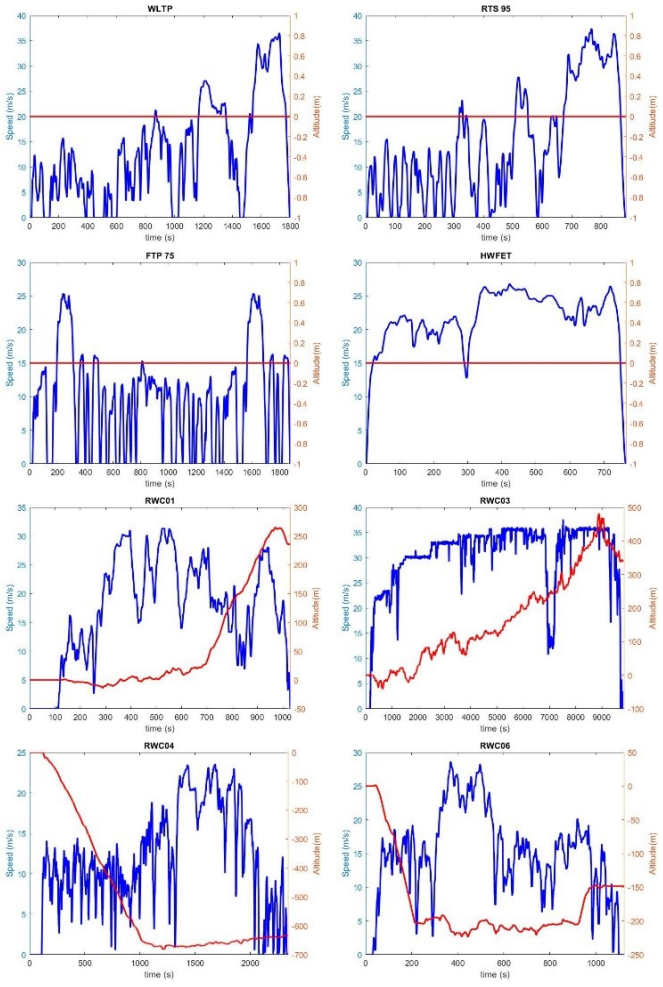

Figure 5. Time series of vehicle speed and net road altitude for retained real-world driving missions.

Table 5. Driving mission characteristics.

Driving mission	Distance (m)	Difference of altitude end-beginning (m)	Maximum speed (km/h)	Total time (s)
WLTP	23.27	0	131.30	1˙800
RTS 95	12.93	0	134.45	886
FTP 75	17.77	0	91.25	1˙877
HWFET	16.49	0	96.30	765
RWC01	17.78	235	112.68	1˙031
RWC03	296	341	135.40	9˙792
RWC04	27.39	-632	84.88	2˙345
RWC06	16.69	-148	102.97	1˙123

Several reasonable and likely values of ambient temperature T_a, namely -5°C, 0°C, 5°C, 10°C, 15°C, 20°C, 25°C, 30°C and 35°C are considered. Ambient temperature might still have a great impact on battery thermal state even if the intervention of battery thermal management system was considered.

Two distinct payloads are considered corresponding to the extreme cases of number of passengers. The vehicle curb weight plus the driver and few equipment involves setting the value n_{pass} to 1, while the fully loaded vehicle condition is associated to setting n_{pass} equal to 5. Varying the payload level might entail different power request and torque split among powertrain components, thus impacting on battery ageing.

Results

This section illustrates HEV simulation results in the different operating conditions listed above to assess the predicted battery lifetime. For each possible use case that represents a combination of driving mission, ambient temperature and payload level, the corresponding battery kilometrical lifetime $L_{bat,km}$ is evaluated. The corresponding use case is then marked as critical in case the predicted battery lifetime is lower than 200 thousand km. Use cases where battery temperature exceeds reasonable limits of 15°C to 35°C are signalized as well.

Obtained simulations results are reported in Table 6, including predicted battery lifetime and minimum and maximum battery temperatures as achieved for each possible driving mission. Critical use cases are underlined, whereas empty cells correspond to those values not evaluable with the cycle aging model adopted. In fact, when battery temperature mainly remains below 15°C, the previously mentioned throughput-based battery capacity fade model cannot be used. This occurs for the RWC03 at -5°C, 0°C and 5°C. By examining more in detail the simulations of the aforesaid driving cycle, it can be understood why this is the only mission implying battery temperature lower than 15°C. RWC03 travels the longest distance (i.e. 296 km), and related time series for ICE state, battery temperature and battery SOC are illustrated in Figure 6 when the ambient temperature is set to -5° C. After a first portion of the driving mission operated in pure electric mode until SOC=0.3 (i.e. around 1600 s), a long charge sustaining phase follows. In this latter condition, the designed RB controller alternates portions travelled in HEV mode (where the SOC descends slowly up to 0.25) to portions travelled in E-save (in which the battery is charged back to 0.30 SOC). The overall employment of the battery while travelling the RWC03 is therefore reduced.

Table 6. Battery sensitivity analysis results.

Driving mission	Variable	n_{pass}	T_a (°C)								
			-5	0	5	10	15	20	25	30	35
WLTP	$L_{bat,km}$ (10^3 km)	1	729	678	622	560	629	424	289	199	139
		5	670	626	578	525	601	406	277	191	133
	T_{max} (°C)	1	20	20	20	20	16.7	21.4	26.3	31.2	36.1
		5	20	20	20	20.2	16.9	21.6	26.5	31.4	36.3
	T_{min} (°C)	1	17.8	18.4	19	19.5	15	20	25	30	35
		5	17.9	18.6	19.2	19.6	15	20	25	30	35
RTS 95	$L_{bat,km}$ (10^3 km)	1	477	457	433	404	486	331	227	158	111
		5	433	417	398	375	463	317	218	152	107
	T_{max} (°C)	1	20	20.2	20.6	21	17	21.7	26.6	31.5	36.4
		5	20.2	20.5	20.9	21.3	17.3	22	26.8	31.7	36.6
	T_{min} (°C)	1	19.4	19.7	19.9	20	15	20	25	30	35
		5	19.6	19.8	20	20	15	20	25	30	35
FTP 75	$L_{bat,km}$ (10^3 km)	1	631	593	549	501	580	390	265	182	127
		5	576	543	506	464	547	369	251	173	120
	T_{max} (°C)	1	20	20	20	20	16.1	21	25.9	31	35.7
		5	20	20	20	20	16.4	21.2	26.1	31	35.9
	T_{min} (°C)	1	17.1	17.9	18.6	19.3	15	20	25	30	35
		5	17.3	18.1	18.9	19.5	15	20	25	30	35
HWFET	$L_{bat,km}$ (10^3 km)	1	654	613	564	506	554	373	254	175	122
		5	521	598	552	496	547	368	251	173	120
	T_{max} (°C)	1	20	20	20.1	20.4	16.2	21	26	30.9	35.8
		5	20	20	20.1	20.5	16.3	21.2	26.1	31	35.9
	T_{min} (°C)	1	19.4	19.7	19.8	20	15	20	25	30	35
		5	19.5	19.8	19.9	20	15	20	25	30	35
RWC01	$L_{bat,km}$ (10^3 km)	1	561	531	495	453	518	352	241	167	117
		5	521	496	465	429	500	341	234	163	114
	T_{max} (°C)	1	20	20.2	20.6	21.1	17.3	22	26.8	31.7	36.5
		5	20.1	20.5	20.9	21.3	17.5	22.2	27.1	31.9	36.7
	T_{min} (°C)	1	19.5	19.6	19.7	19.9	15	20	25	30	35
		5	19.5	19.7	19.8	19.9	15	20	25	30	35
RWC03	$L_{bat,km}$ (10^3 km)	1				3168	3335	2269	1552	1077	755
		5				2680	2812	1921	1319	919	647
	T_{max} (°C)	1	20	20.2	20.8	21.5	18.2	22.8	27.8	32.5	37.2
		5	20	20.3	21	21.7	18.4	23.1	27.9	32.6	37.4
	T_{min} (°C)	1	7.9	10.7	13.6	16.4	15	20	25	30	35
		5	8.9	11.7	14.5	17.3	15	20	25	30	35
RWC04	$L_{bat,km}$ (10^3 km)	1	827	764	697	626	705	476	324	223	155
		5	753	698	639	577	656	443	302	209	146
	T_{max} (°C)	1	20	20	20	20	16.5	21.3	26.2	31.1	36
		5	20	20	20	20	16.9	21.6	26.5	31.4	36.3
	T_{min} (°C)	1	16.7	17.6	18.5	19.3	15	20	25	30	35
		5	16.9	17.9	18.8	19.3	15	20	25	30	35
RWC06	$L_{bat,km}$ (10^3 km)	1	611	579	541	497	577	391	267	184	129
		5	578	551	518	479	567	385	263	182	127
	T_{max} (°C)	1	20	20	20.1	20.5	16.6	21.4	26.3	31.2	36.1
		5	20	20	20.2	20.6	16.8	21.6	26.5	31.3	36.2
	T_{min} (°C)	1	19	19.5	19.7	19.9	15	20	25	30	35
		5	19.2	19.6	19.8	19.9	15	20	25	30	35

Explanation for RWC03 always guaranteeing a battery lifetime larger than 200 thousand km independently on ambient temperature can be provided in this way. After the initial charge depleting phase, in which intense Joule's heat is generated, the battery temperature dramatically drops in RWC03, because the battery pack is employed less. Indeed, traction is mainly provided by the ICE, and the passive cooling due to the surrounding air is no more balanced by the internal generation of heat.

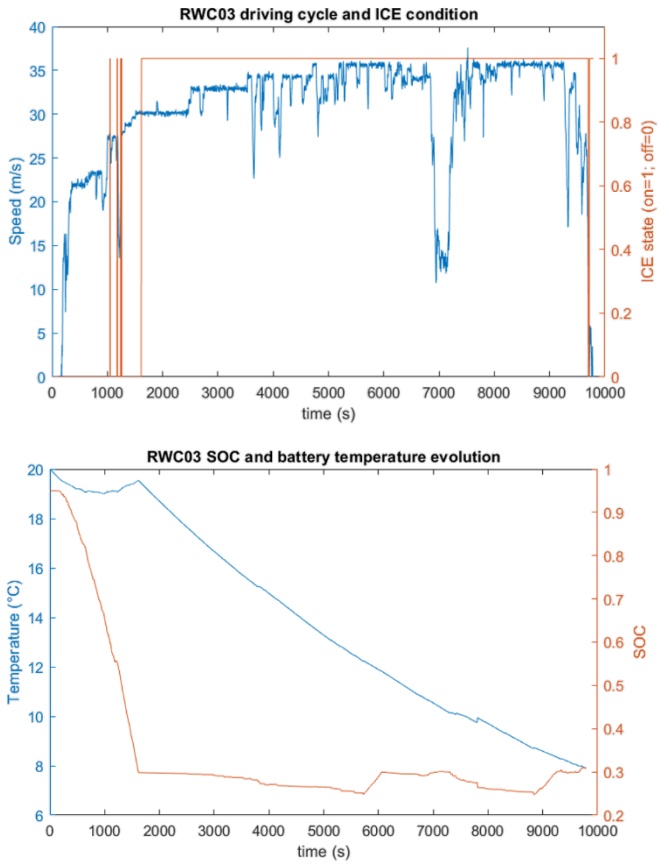

Figure 6. Time series of ICE state, battery temperature and SOC for RWC03 simulated at -5°C ambient temperature.

Moving to the simulations conducted at high temperatures, completely different considerations can be drawn. High temperature issues appear indeed more widespread among different driving missions. In some cases the battery is not able to provide a $L_{bat,km}$ higher than 200 thousand km even if the battery temperature never exceeds the upper limit of 35°C. Ambient temperatures higher than 25° C are found notably affecting battery lifetime in this framework. As consequence, an electrified powertrain EMS that is calibrated for 25°C ambient temperature might need re-calibration for higher ambient temperatures, as Table 6 testifies. These results demonstrate how few degrees of temperature variation can considerably undermine battery lifetime. Battery thermal management is confirmed having a key role in electrified vehicles, and battery temperature must be included among the parameters monitored by HEV EMSs.

On their behalf, evaluating the impact of driving conditions and payload level on the battery lifetime appears less intuitive. First, it can be observed that standard drive cycles appear more problematic than RWCs for the retained HEV and on-board RB EMS. This counterintuitive consideration might relate to both specific driving habits considered and to the standard drive cycles involving in general shorter distances driven that involve more frequent battery charging from the grid. Concerning the payload level, when lightly loaded vehicle conditions are considered the HWFET results in general more critical than the FTP 75 from the point of view of predicted battery lifetime as example. However, when fully loaded vehicle conditions are retained, values of predicted battery lifetime for these two driving missions become comparable. Explanation for these outcomes might relate to the propelling power limitation of MGP4. Simulating power demanding driving conditions (e.g. by incrementing n_{pass} or changing the driving mission) might not imply a significative reduction of battery lifetime. On the other hand, an increase in fuel consumption might be observed as the EMS selects HEV operation when the requested power cannot be provided in Electric mode. In general, these results corroborate the need of considering a large number of different use cases by varying both payload level and driving conditions when dealing with high ambient temperatures.

Conclusions

This paper aims at illustrating the importance that a plausible thermal model of the battery holds for evaluating the actual ageing rate of a PHEV ESS during the quasi-static simulation of different driving missions at different payload levels and ambient temperatures. In fact, in accordance with the cycle life model here adopted [11], slight differences in battery operating temperature might already imply a notable acceleration in battery ageing. Consequently, including battery temperature in HEV EMS becomes necessary in order to safeguard HV battery life. However, although this outcome could sound particularly disturbing, it must not be forgotten that the adopted cycle ageing model extends over a rather ample thermal range (15°C-60°C) and, therefore, could be inaccurate when evaluating modest variations of Celsius degrees, as indeed done in this work. Moreover, it must also be remembered that the afore-said life model refers to a specific commercial type of Li-ion cell (A123 ANR26650); consequently, the results here attained cannot be ascribed directly to Li-ion batteries in general, although a similar behavior can be certainly expected [2,16]. Finally, although partially debated here, it would be undoubtedly interesting to thoroughly inspect battery operation at low temperatures as well, so as to conduct a complete treatise of this thermal range too. With respect to the fact of considering several driving missions and load conditions, these aspects have less impact than temperature, but variating them in accordance with expected vehicle uses can allow to conduct a complete examination of battery cycle ageing.

References

1. European Parliament, "Electric road vehicles in the European Union: Trends, impacts and policies". https://www.europarl.europa.eu/RegData/etudes/BRIE/2019/637895/EPRS_BRI(2019)637895_EN.pdf, accessed Oct. 2020.
2. Emadi, A., "Advanced Electric Drive Vehicles", (CRC Press, Taylor & Francis Group, LLC, 2015), 1-26 and 187-282, ISBN: 978-1-4665-9770-9.
3. Bloom, I., Cole, B. W., Sohn, J. J., Jones, S. A., Polzin, E. G., Battaglia, V. S., Henriksen, G. L., Motloch, C., Richardson, R., Unkelhaeuser, T., Ingersoll, D., and Case, H. L., "An accelerated calendar and cycle life study of Li-ion cells," Journal of Power Sources, vol. 101, no. 2, 238–247, Oct. 2001, doi: 10.1016/S0378-7753(01)00783-2.

4. Ebbesen, S., Elbert, P., and Guzzella, L., "Battery State-of-Health Perceptive Energy Management for Hybrid Electric Vehicles," IEEE Transactions on Vehicular Technology, vol. 61, no. 7, 2893-2900, Sept. 2012, doi: 10.1109/TVT.2012.2203836.
5. Anselma, P., Kollmeyer, P., Belingardi, G., and Emadi, A., "Multitarget Evaluation of Hybrid Electric Vehicle Powertrain Architectures Considering Fuel Economy and Battery Lifetime," SAE Technical Paper 2020-37-0015, 2020, doi: 10.4271/2020-37-0015.
6. Anselma, P. and Belingardi, G., "Next Generation HEV Powertrain Design Tools: Roadmap and Challenges," SAE Technical Paper 2019-01-2602, 2019, doi: 10.4271/2019-01-2602.
7. Fiat Chrysler Automobiles, "Renegade 4xe and Compass 4xe: the Jeep® brand's take on the plug-in hybrid," http://www.media.fcaemea.com/em-en/jeep/press/renegade-4xe-and-compass-4xe-the-jeep-brand-s-take-on-the-plug-in-hybrid, accessed Oct. 2020.
8. Ronghua, D., Xiaosong, H., Shaobo, X., Lin, H., Zhiyong, Z., and Xianke, L., "Battery aging-and temperature-aware predictive energy management for hybrid electric vehicles," Journal of Power Sources, vol. 473, Oct. 2020, doi: 10.1016/j.jpowsour.2020.228568.
9. Miro Padovani, T., Debert, M., Colin, G., and Chamaillard, Y., "Optimal energy management strategy including battery health through thermal management for hybrid vehicles," IFAC Proceedings Volumes, vol. 46, no. 21, 384-389, 2013, doi: 10.3182/20130904-4-JP-2042.00137.
10. A123 Systems, "Nanophosphate® High Power Lithium Ion Cell ANR26650M1-B," https://www.batteryspace.com/prod-specs/6610.pdf, accessed Oct. 2020.
11. Wang, J., Liu, P., Hicks-Garner, J., Sherman, E., Soukiazian, S., Verbrugge, M., Tataria, H., Musser, J., and Finamore, P., "Cycle-life model for graphite- LiFePO4 cells," Journal of Power Sources, vol. 196, no. 8, 3942– 3948, April 2011, doi: 10.1016/j.jpowsour.2010.11.134.
12. Alix, G., Dabadie, J., and Font, G., "An ICE Map Generation Tool Applied to the Evaluation of the Impact of Downsizing on Hybrid Vehicle Consumption," SAE Technical Paper 2015-24-2385, 2015, doi: 10.4271/2015-24-2385.
13. Le Berr, F., Abdelli, A., Postariu, D.-M., and Benlamine, R., "Design and Optimization of Future Hybrid and Electric Propulsion Systems: An Advanced Tool Integrated in a Complete Workflow to Study Electric Devices", Oil Gas Sci. Technol., vol. 67, no. 4, 547-562, 2012, doi: 10.2516/ogst/2012029.
14. United States Environmental Protection Agency, "Compliance and Fuel Economy Data -Annual Certification Data for Vehicles, Engines, and Equipment," https://www.epa.gov/compliance-and-fuel-economy-data/annual-certification-data-vehicles-engines-and-equipment, accessed Oct. 2020.
15. Li, Q., Itoh, Y., Imanishi, N., Hirano, A., Takeda, Y., and Yamamoto, O., "All solid lithium polymer batteries with a novel composite polymer electrolyte," Solid State Ion., vol. 159, 97–109, March 2003, doi: 10.1016/S0167-2738(03)00004-3.
16. Vidal, C., Gross, O., Gu, R., Kollmeyer, P., and Emadi, A., "xEV Li-Ion Battery Low-Temperature Effects - Review," in IEEE Transactions on Vehicular Technology, vol. 68, no. 5, 4560-4572, 2019, doi: 10.1109/TVT.2019.2906487.
17. De Vita, A., Maheshwari, A., Destro, M., Santarelli, M., and Carello, M., "Transient thermal analysis of a lithium-ion battery pack comparing different cooling solutions for automotive applications," Applied Energy, Elsevier, vol. 206(C), 101-112, Nov. 2017, doi: 10.1016/j.apenergy.2017.08.184.
18. Onori, S., Spagnol, P., Marano, V., Guezennec, Y., and Rizzoni, G., "A new life estimation method for lithium–ion batteries in plug–in hybrid electric vehicles applications," Int. J. Power Electron., vol. 4, no. 3, 302–319, 2012, doi: 10.1504/IJPELEC.2012.046609.

Contact Information

Marco Del Prete, **Pier Giuseppe Anselma**
Department of Mechanical and Aerospace Engineering (DIMEAS), Center for Automotive Research and Sustainable Mobility (CARS), Politecnico di Torino, Corso Duca degli Abruzzi 24, 10129 Torino, Italy.
marco.delprete@studenti.polito.it, pier.anselma@polito.it

Definitions/Abbreviations

BEV	battery electric vehicle
DOD	depth-of-discharge
ECM	equivalent circuit model
EMS	energy management strategy
EOL	end of life
ESS	energy storage system
FTP 75	Federal Test Procedure 75 driving cycle
HEV	hybrid electric vehicle
HV	high-voltage
HWFET	Highway Fuel Economy Test driving cycle
ICE	internal combustion engine
MGP0	electric motor/generator in configuration P0
MGP4	electric motor/generator in configuration P4
PHEV	plug-in hybrid electric vehicle
QSA	quasi-static approach
RB	rule-based
RTS 95	random test standardized 95 driving cycle
RWC	real world driving cycle
SOC	state-of-charge
SOH	state-of-health
WLTP	Worldwide-harmonized Light Vehicle Test procedure